ρ0 photoproduction in ultraperipheral relativistic heavy ion collisions at √sNN=200 GeV

(STAR Collaboration) Abelev, B. I.; ...; Planinić, Mirko; ...; Poljak, Nikola; ...; Zuo, J. X.

Journal article, Published version
Rad u časopisu, Objavljena verzija rada (izdavačev PDF)

Permanent link / Trajna poveznica: https://urn.nsk.hr/urn:nbn:hr:217:269837

Download date / Datum preuzimanja: **2024-11-23**

Repository / Repozitorij:

Repository of the Faculty of Science - University of Zagreb

ρ^0 photoproduction in ultraperipheral relativistic heavy ion collisions at $\sqrt{s_{NN}} = 200$ GeV

B. I. Abelev,[10] M. M. Aggarwal,[32] Z. Ahammed,[47] B. D. Anderson,[21] D. Arkhipkin,[14] G. S. Averichev,[13] Y. Bai,[30]
J. Balewski,[18] O. Barannikova,[10] L. S. Barnby,[2] J. Baudot,[19] S. Baumgart,[52] D. R. Beavis,[3] R. Bellwied,[50] F. Benedosso,[30]
R. R. Betts,[10] S. Bhardwaj,[37] A. Bhasin,[20] A. K. Bhati,[32] H. Bichsel,[49] J. Bielcik,[12] J. Bielcikova,[12] L. C. Bland,[3] S.-L. Blyth,[24]
M. Bombara,[2] B. E. Bonner,[38] M. Botje,[30] J. Bouchet,[42] E. Braidot,[30] A. V. Brandin,[28] S. Bueltmann,[3] T. P. Burton,[2]
M. Bystersky,[12] X. Z. Cai,[41] H. Caines,[52] M. Calderón de la Barca Sánchez,[6] J. Callner,[10] O. Catu,[52] D. Cebra,[6]
M. C. Cervantes,[43] Z. Chajecki,[31] P. Chaloupka,[12] S. Chattopadhyay,[47] H. F. Chen,[40] J. H. Chen,[41] J. Y. Chen,[51] J. Cheng,[45]
M. Cherney,[11] A. Chikanian,[52] K. E. Choi,[36] W. Christie,[3] S. U. Chung,[3] R. F. Clarke,[43] M. J. M. Codrington,[43] J. P. Coffin,[19]
T. M. Cormier,[50] M. R. Cosentino,[39] J. G. Cramer,[49] H. J. Crawford,[5] D. Das,[6] S. Dash,[16] M. Daugherity,[44] M. M. de Moura,[39]
T. G. Dedovich,[13] M. DePhillips,[3] A. A. Derevschikov,[34] R. Derradi de Souza,[8] L. Didenko,[3] T. Dietel,[15] P. Djawotho,[18]
S. M. Dogra,[20] X. Dong,[24] J. L. Drachenberg,[43] J. E. Draper,[6] F. Du,[52] J. C. Dunlop,[3] M. R. Dutta Mazumdar,[47]
W. R. Edwards,[24] L. G. Efimov,[13] E. Elhalhuli,[2] V. Emelianov,[28] J. Engelage,[5] G. Eppley,[38] B. Erazmus,[42] M. Estienne,[19]
L. Eun,[33] P. Fachini,[3] R. Fatemi,[22] J. Fedorisin,[13] A. Feng,[51] P. Filip,[14] E. Finch,[52] V. Fine,[3] Y. Fisyak,[3] J. Fu,[51]
C. A. Gagliardi,[43] L. Gaillard,[2] M. S. Ganti,[47] E. Garcia-Solis,[10] V. Ghazikhanian,[7] P. Ghosh,[47] Y. N. Gorbunov,[11] A. Gordon,[3]
O. Grebenyuk,[30] D. Grosnick,[46] B. Grube,[36] S. M. Guertin,[7] K. S. F. F. Guimaraes,[39] A. Gupta,[20] N. Gupta,[20] W. Guryn,[3]
B. Haag,[6] T. J. Hallman,[3] A. Hamed,[43] J. W. Harris,[52] W. He,[18] M. Heinz,[52] T. W. Henry,[43] S. Hepplemann,[33] B. Hippolyte,[19]
A. Hirsch,[35] E. Hjort,[24] A. M. Hoffman,[25] G. W. Hoffmann,[44] D. J. Hofman,[10] R. S. Hollis,[10] M. J. Horner,[24] H. Z. Huang,[7]
E. W. Hughes,[4] T. J. Humanic,[31] G. Igo,[7] A. Iordanova,[10] P. Jacobs,[24] W. W. Jacobs,[18] P. Jakl,[12] F. Jin,[41] P. G. Jones,[2]
E. G. Judd,[5] S. Kabana,[42] K. Kajimoto,[44] K. Kang,[45] J. Kapitan,[12] M. Kaplan,[9] D. Keane,[21] A. Kechechyan,[13] D. Kettler,[49]
V. Yu. Khodyrev,[34] J. Kiryluk,[24] A. Kisiel,[31] S. R. Klein,[24] A. G. Knospe,[52] A. Kocoloski,[25] D. D. Koetke,[46] T. Kollegger,[15]
M. Kopytine,[21] L. Kotchenda,[28] V. Kouchpil,[12] K. L. Kowalik,[24] P. Kravtsov,[28] V. I. Kravtsov,[34] K. Krueger,[1] C. Kuhn,[19]
A. Kumar,[32] P. Kurnadi,[7] M. A. C. Lamont,[3] J. M. Landgraf,[3] S. Lange,[15] S. LaPointe,[50] F. Laue,[3] J. Lauret,[3] A. Lebedev,[3]
R. Lednicky,[14] C.-H. Lee,[36] M. J. LeVine,[3] C. Li,[40] Q. Li,[50] Y. Li,[45] G. Lin,[52] X. Lin,[51] S. J. Lindenbaum,[29] M. A. Lisa,[31]
F. Liu,[51] H. Liu,[40] J. Liu,[38] L. Liu,[51] T. Ljubicic,[3] W. J. Llope,[38] R. S. Longacre,[3] W. A. Love,[3] Y. Lu,[40] T. Ludlam,[3] D. Lynn,[3]
G. L. Ma,[41] J. G. Ma,[7] Y. G. Ma,[41] D. P. Mahapatra,[16] R. Majka,[52] L. K. Mangotra,[20] R. Manweiler,[46] S. Margetis,[21]
C. Markert,[44] H. S. Matis,[24] Yu. A. Matulenko,[34] T. S. McShane,[11] A. Meschanin,[34] J. Millane,[25] M. L. Miller,[25]
N. G. Minaev,[34] S. Mioduszewski,[43] A. Mischke,[30] J. Mitchell,[38] B. Mohanty,[47] D. A. Morozov,[34] M. G. Munhoz,[39]
B. K. Nandi,[17] C. Nattrass,[52] T. K. Nayak,[47] J. M. Nelson,[2] C. Nepali,[21] P. K. Netrakanti,[35] M. J. Ng,[5] L. V. Nogach,[34]
S. B. Nurushev,[34] G. Odyniec,[24] A. Ogawa,[3] H. Okada,[3] V. Okorokov,[28] D. Olson,[24] M. Pachr,[12] S. K. Pal,[47] Y. Panebratsev,[13]
A. I. Pavlinov,[50] T. Pawlak,[48] T. Peitzmann,[30] V. Perevoztchikov,[3] C. Perkins,[5] W. Peryt,[48] S. C. Phatak,[16] M. Planinic,[53]
J. Pluta,[48] N. Poljak,[53] N. Porile,[35] A. M. Poskanzer,[24] M. Potekhin,[3] B. V. K. S. Potukuchi,[20] D. Prindle,[49] C. Pruneau,[50]
N. K. Pruthi,[32] J. Putschke,[52] I. A. Qattan,[18] R. Raniwala,[37] S. Raniwala,[37] R. L. Ray,[44] D. Relyea,[4] A. Ridiger,[28] H. G. Ritter,[24]
J. B. Roberts,[38] O. V. Rogachevskiy,[13] J. L. Romero,[6] A. Rose,[24] C. Roy,[42] L. Ruan,[3] M. J. Russcher,[30] V. Rykov,[21] R. Sahoo,[42]
I. Sakrejda,[24] T. Sakuma,[25] S. Salur,[52] J. Sandweiss,[52] M. Sarsour,[43] J. Schambach,[44] R. P. Scharenberg,[35] N. Schmitz,[26]
J. Seger,[11] I. Selyuzhenkov,[50] P. Seyboth,[26] A. Shabetai,[19] E. Shahaliev,[13] M. Shao,[40] M. Sharma,[32] X.-H. Shi,[41]
E. P. Sichtermann,[24] F. Simon,[26] R. N. Singaraju,[47] M. J. Skoby,[35] N. Smirnov,[52] R. Snellings,[30] P. Sorensen,[3] J. Sowinski,[18]
J. Speltz,[19] H. M. Spinka,[1] B. Srivastava,[35] A. Stadnik,[13] T. D. S. Stanislaus,[46] D. Staszak,[7] R. Stock,[15] M. Strikhanov,[28]
B. Stringfellow,[35] A. A. P. Suaide,[39] M. C. Suarez,[10] N. L. Subba,[21] M. Sumbera,[12] X. M. Sun,[24] Z. Sun,[23] B. Surrow,[25]
T. J. M. Symons,[24] A. Szanto de Toledo,[39] J. Takahashi,[8] A. H. Tang,[3] Z. Tang,[40] T. Tarnowsky,[35] D. Thein,[44] J. H. Thomas,[24]
J. Tian,[41] A. R. Timmins,[2] S. Timoshenko,[28] M. Tokarev,[13] T. A. Trainor,[49] V. N. Tram,[24] A. L. Trattner,[5] S. Trentalange,[7]
R. E. Tribble,[43] O. D. Tsai,[7] J. Ulery,[35] T. Ullrich,[3] D. G. Underwood,[1] G. Van Buren,[3] N. van der Kolk,[30] M. van Leeuwen,[24]
A. M. Vander Molen,[27] R. Varma,[17] G. M. S. Vasconcelos,[8] I. M. Vasilevski,[14] A. N. Vasiliev,[34] R. Vernet,[19] F. Videbaek,[3]
S. E. Vigdor,[18] Y. P. Viyogi,[16] S. Vokal,[13] S. A. Voloshin,[50] M. Wada,[44] W. T. Waggoner,[11] F. Wang,[35] G. Wang,[7] J. S. Wang,[23]
Q. Wang,[35] X. Wang,[45] X. L. Wang,[40] Y. Wang,[45] J. C. Webb,[46] G. D. Westfall,[27] C. Whitten Jr.,[7] H. Wieman,[24]
S. W. Wissink,[18] R. Witt,[52] J. Wu,[40] Y. Wu,[51] N. Xu,[24] Q. H. Xu,[24] Z. Xu,[3] P. Yepes,[38] I.-K. Yoo,[36] Q. Yue,[45] M. Zawisza,[48]
H. Zbroszczyk,[48] W. Zhan,[23] H. Zhang,[3] S. Zhang,[41] W. M. Zhang,[21] Y. Zhang,[40] Z. P. Zhang,[40] Y. Zhao,[40] C. Zhong,[41]
J. Zhou,[38] R. Zoulkarneev,[14] Y. Zoulkarneeva,[14] and J. X. Zuo[41]

(STAR Collaboration)

[1]*Argonne National Laboratory, Argonne, Illinois 60439, USA*
[2]*University of Birmingham, Birmingham, United Kingdom*
[3]*Brookhaven National Laboratory, Upton, New York 11973, USA*
[4]*California Institute of Technology, Pasadena, California 91125, USA*
[5]*University of California, Berkeley, California 94720, USA*
[6]*University of California, Davis, California 95616, USA*
[7]*University of California, Los Angeles, California 90095, USA*
[8]*Universidade Estadual de Campinas, Sao Paulo, Brazil*
[9]*Carnegie Mellon University, Pittsburgh, Pennsylvania 15213, USA*

[10]*University of Illinois at Chicago, Chicago, Illinois 60607, USA*
[11]*Creighton University, Omaha, Nebraska 68178, USA*
[12]*Nuclear Physics Institute AS CR, 250 68 Řež, Prague, Czech Republic*
[13]*Laboratory for High Energy (JINR), Dubna, Russia*
[14]*Particle Physics Laboratory (JINR), Dubna, Russia*
[15]*University of Frankfurt, Frankfurt, Germany*
[16]*Institute of Physics, Bhubaneswar 751005, India*
[17]*Indian Institute of Technology, Mumbai, India*
[18]*Indiana University, Bloomington, Indiana 47408, USA*
[19]*Institut de Recherches Subatomiques, Strasbourg, France*
[20]*University of Jammu, Jammu 180001, India*
[21]*Kent State University, Kent, Ohio 44242, USA*
[22]*University of Kentucky, Lexington, Kentucky 40506-0055, USA*
[23]*Institute of Modern Physics, Lanzhou, China*
[24]*Lawrence Berkeley National Laboratory, Berkeley, California 94720, USA*
[25]*Massachusetts Institute of Technology, Cambridge, Massachusetts 02139-4307, USA*
[26]*Max-Planck-Institut für Physik, Munich, Germany*
[27]*Michigan State University, East Lansing, Michigan 48824, USA*
[28]*Moscow Engineering Physics Institute, Moscow, Russia*
[29]*City College of New York, New York City, New York 10031, USA*
[30]*NIKHEF and Utrecht University, Amsterdam, The Netherlands*
[31]*Ohio State University, Columbus, Ohio 43210, USA*
[32]*Panjab University, Chandigarh 160014, India*
[33]*Pennsylvania State University, University Park, Pennsylvania 16802, USA*
[34]*Institute of High Energy Physics, Protvino, Russia*
[35]*Purdue University, West Lafayette, Indiana 47907, USA*
[36]*Pusan National University, Pusan, Republic of Korea*
[37]*University of Rajasthan, Jaipur 302004, India*
[38]*Rice University, Houston, Texas 77251, USA*
[39]*Universidade de Sao Paulo, Sao Paulo, Brazil*
[40]*University of Science & Technology of China, Hefei 230026, China*
[41]*Shanghai Institute of Applied Physics, Shanghai 201800, China*
[42]*SUBATECH, Nantes, France*
[43]*Texas A&M University, College Station, Texas 77843, USA*
[44]*University of Texas, Austin, Texas 78712, USA*
[45]*Tsinghua University, Beijing 100084, China*
[46]*Valparaiso University, Valparaiso, Indiana 46383, USA*
[47]*Variable Energy Cyclotron Centre, Kolkata 700064, India*
[48]*Warsaw University of Technology, Warsaw, Poland*
[49]*University of Washington, Seattle, Washington 98195, USA*
[50]*Wayne State University, Detroit, Michigan 48201, USA*
[51]*Institute of Particle Physics, CCNU (HZNU), Wuhan 430079, China*
[52]*Yale University, New Haven, Connecticut 06520, USA*
[53]*University of Zagreb, Zagreb HR-10002, Croatia*

Photoproduction reactions occur when the electromagnetic field of a relativistic heavy ion interacts with another heavy ion. The STAR Collaboration presents a measurement of ρ^0 and direct $\pi^+\pi^-$ photoproduction in ultraperipheral relativistic heavy ion collisions at $\sqrt{s_{NN}} = 200$ GeV. We observe both exclusive photoproduction and photoproduction accompanied by mutual Coulomb excitation. We find a coherent cross section of $\sigma(\text{AuAu} \rightarrow \text{Au}^*\text{Au}^*\rho^0) = 530 \pm 19(\text{stat.}) \pm 57(\text{syst.})$ mb, in accord with theoretical calculations based on a Glauber approach, but considerably below the predictions of a color dipole model. The ρ^0 transverse momentum spectrum (p_T^2) is fit by a double exponential curve including both coherent and incoherent coupling to the target nucleus; we find $\sigma_{\text{inc}}/\sigma_{\text{coh}} = 0.29 \pm 0.03$ (stat.) ± 0.08 (syst.). The ratio of direct $\pi^+\pi^-$ to ρ^0 production is comparable to that observed in γp collisions at HERA and appears to be independent of photon energy. Finally, the measured ρ^0 spin helicity matrix elements agree within errors with the expected s-channel helicity conservation.

I. INTRODUCTION

In heavy ion collisions when the electromagnetic field of one nucleus interacts with another nucleus, photoproduction can occur [1,2]. Photoproduction is visible in ultraperipheral collisions (UPCs), which occur when the impact parameter b is more than twice the nuclear radius R_A, so no hadronic interactions are present. The electromagnetic field of a relativistic nucleus may be represented as a flux of almost-real virtual photons, following the Weizsäcker-Williams method [3]. In this framework, the physics of the interactions between particles is equivalent to that of the interactions between photons and particles. The photon flux scales as the square of the nuclear charge and so the cross sections can be large in heavy ion interactions.

Photoproduction of ρ^0s occurs when a photon from one nucleus fluctuates to a quark-antiquark pair, which then scatters elastically from the other nucleus, emerging as a ρ^0. The elastic scattering can be treated as being due to Pomeron exchange [4].

The cross section for ρ^0 production depends on the $q\bar{q}$ coupling to the nuclear target. For ρ^0 production at large transverse momentum, p_T, the $q\bar{q}$ pair couples to the individual nucleons. The incoherent cross section scales roughly as the atomic number A, minus a correction from nuclear absorption of the ρ^0.

At smaller p_T, roughly $p_T < \hbar/R_A$, the $q\bar{q}$ pair couples coherently to the entire nucleus; naively, this leads to a cross section that scales as A^2. The coherent production is regulated by the nuclear form factor $F(t)$, so ρ^0 photoproduction is sensitive to the ρ^0-nucleon interaction cross section and the nuclear structure functions [2].

There are three published calculations of the coherent ρ^0 photoproduction cross section in heavy ion collisions. The first model (Klein and Nystrand—KN) uses vector meson dominance (VMD) plus a classical mechanical Glauber approach for nuclear scattering. KN uses information from the $\gamma p \rightarrow V p$ experiments for extrapolation [5]. The model predicts a total coherent ρ^0 photoproduction cross section of $\sigma_{\rho^0} = 590$ mb in gold-gold collisions at $\sqrt{s_{NN}} = 200$ GeV. The second model (Frankfurt, Strikman, and Zhalov—FSZ) treats the ρ^0 production by using the generalized quantum VMD and the QCD Gribov-Glauber approach [6,7]; it predicts $\sigma_{\rho^0} = 934$ mb [7], about 60% higher than that from the KN model, but with a similar rapidity distribution. The third model (Goncalves and Machado—GM) describes the photoproduction of the vector mesons in UPC events using the QCD color dipole approach [8]. This model includes nuclear effects and parton saturation phenomena. It finds $\sigma_{\rho^0} = 876$ mb, with a rapidity distribution very different from that of the other models. The FSZ and GM models provide predictions for the momentum transfer dependence of both coherent and incoherent ρ^0 production.

The ρ^0 photoproduction on nuclear targets has been studied at fixed-target experiments [9] and at RHIC (Relativistic Heavy Ion Collider). Previous fixed-target photoproduction experiments with nuclear targets were done at relatively low collision energies [9]. The PHENIX Collaboration has studied J/ψ photoproduction [10] in heavy ion interactions at RHIC.

The Solenoidal Tracker at RHIC (STAR) Collaboration has published measurements of the ρ^0 production cross section at a center-of-mass energy of $\sqrt{s_{NN}} = 130$ GeV per nucleon pair [11]. This work presents results at a higher center-of-mass energy of $\sqrt{s_{NN}} = 200$ GeV. To produce a meson with mass m_{ρ^0} at rapidity y_{ρ^0} a minimum photon-nucleon center-of-mass energy of $W_{\gamma N} = [\sqrt{s_{NN}} m_{\rho^0} \exp(y_{\rho^0})]^{1/2}$ is required. At mid-rapidity this corresponds to about 12.5 GeV, and in the region $|y_{\rho^0}| < 1$ to a range of $7.6 < W_{\gamma N} < 20.6$ GeV, which is well above that of previous fixed-target photoproduction experiments [9].

The γ-nucleon collision energy is related to a minimum photon energy in the laboratory frame, which is given by

$$E_\gamma = \frac{m_{\rho^0}}{2} \exp(\pm y_{\rho^0}). \tag{1}$$

The two signs reflect the ambiguity about which nucleus emits the photon.

In the rest frame of the target nucleus, the minimum photon energy is $2\gamma_L$ times higher than in the laboratory frame, where γ_L is the Lorentz boost of the beam. For $\sqrt{s_{NN}} = 200$ GeV, γ_L is about 108; at mid-rapidity, this corresponds to a photon energy in the target frame of about 84 GeV. For nonzero rapidities, most of the ρ^0 production comes from the solution with the lowest energy, so the minimum energy required is even less. To evaluate whether or not the ρ^0s can be produced coherently, one must compare this energy to the maximum photon energy. In the rest frame of the target nucleus, this maximum is determined by the uncertainty relation $E_\gamma^{\text{target}} \lesssim (2\gamma_L^2 - 1)\hbar/R_A$. For $\gamma_L = 108$, this maximum is approximately 650 GeV. Since the minimal energy required to produce a ρ^0 is much less than 650 GeV, we expect to easily observe coherently produced ρ^0 mesons.

In this study, we have collected data at higher energy ($\sqrt{s_{NN}} = 200$ GeV versus $\sqrt{s_{NN}} = 130$ GeV) and with about 10 times more statistics than the previous STAR study, allowing for more precise measurements of the cross section. We have extended the previous analysis by measuring both the coherent and incoherent contributions to the photoproduction cross section and we have also measured the spin-matrix elements for ρ^0 production. In addition to exclusive ρ^0 photoproduction, we have studied ρ^0 photoproduction accompanied by mutual Coulomb excitation, as is shown in Fig. 1. This process primarily occurs via three-photon exchange, with one photon producing the ρ^0, and one photon exciting each
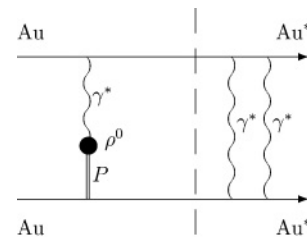

FIG. 1. The diagram for ρ^0 photoproduction accompanied by mutual Coulomb excitation. The latter process proceeds by mutual photon exchange; the vertical dashed line shows how the photoproduction factorizes from the mutual Coulomb excitation.

nucleus [12,13]. Each single-photon reaction is independent, and the cross sections may be written as an integral over the impact parameter,

$$\sigma(\mathrm{AuAu} \rightarrow \mathrm{Au}^* \mathrm{Au}^* \rho^0)$$
$$= \int d^2 b [1 - P_{\mathrm{Had}}(b)] P_{\rho^0}(b) P_{Xn,1}(b) P_{Xn,2}(b), \quad (2)$$

where $P_{\mathrm{Had}}(b)$ is the probability of a hadronic interaction, $P_{\rho^0}(b)$ is the probability to produce a ρ^0, and $P_{Xn,1}(b)$ and $P_{Xn,2}(b)$ are the probabilities to excite nucleus 1 and 2, respectively. The three-photon exchange reactions are biased toward smaller impact parameters than single-photon reactions, leading to a harder photon spectrum and an altered rapidity distribution. In mutual Coulomb excitation, the nuclei decay primarily by channels involving neutron emission. This is attractive experimentally, because the neutrons provide simple trigger signals that can be detected with the STAR Zero Degree Calorimeters [14].

One particular nuclear excitation merits special interest: electromagnetic excitation to a Giant Dipole Resonance (GDR) [15] of either one or both ions. GDR involves particularly low-energy photons. A single GDR is the main contribution in the total fragmentation cross section induced by Coulomb excitation in UPCs. GDRs usually decay by single-neutron emission, which is considered to be a major source of beam loss in heavy ion colliders [2].

The hypothesis of *s*-channel helicity conservation for vector mesons suggests that the vector meson produced in the collision will retain the helicity of the initial photon [16]. The differential production cross section and the decay angular distribution of the vector meson can be expressed as a function of the vector meson spin density matrix, which is represented by the sum of the helicity states and encompasses transverse and longitudinal elements and their combinations [17]. As a consequence of parity conservation and the symmetry properties of the matrix elements, the decay angular distribution can be greatly simplified. If the helicities are conserved in the hadronic center-of-mass system, there are only three independent helicity amplitudes in the final function [17]. In this paper, we report a measurement of these three ρ^0 spin density matrix elements for $p_T < 150$ MeV/c and a photon-nucleon center-of-mass system energy $W_{\gamma N} \approx 10$ GeV, beyond previous fixed-target experiments [18].

II. EXPERIMENTAL SETUP AND TRIGGERING

This analysis uses data taken with the STAR detector at Brookhaven National Laboratory during the 2001 run. Gold nuclei were collided at $\sqrt{s_{NN}} = 200$ GeV and the charged particle tracks were reconstructed in a cylindrical Time Projection Chamber (TPC) [19]. The TPC is a 4.2-m-long barrel with a 2-m radius operated in a solenoidal magnetic field of 0.5 T. The TPC detected charged tracks with pseudorapidity $|\eta| < 1.2$ and $p_T > 100$ MeV/c with an efficiency of about 85%. The TPC is surrounded by 240 Central Trigger Barrel (CTB) [20] slats, which are plastic scintillator detectors spaced every 6 degrees in Φ with complete (hermetic) coverage over the full range of rapidity covered by the TPC. Two Zero Degree Calorimeters (ZDCs) [14] are situated along the beam pipe at ± 18 m from the interaction point. They have an acceptance close to unity for the neutrons originating from nuclear breakup.

This analysis used data from two triggers: a topology trigger and a minimum bias trigger. The topology trigger divided the CTB detector into four azimuthal quadrants. A coincidence between the left- and right-side quadrants was required, while at the same time the top and bottom quadrants were required to be empty. The veto from the top and bottom quadrants was used to reduce the trigger rate from cosmic rays.

The minimum bias trigger required a coincidence between the two ZDCs and thus was sensitive to photoproduction accompanied by mutual Coulomb excitation. By eliminating cosmic rays and other extraneous interactions, this trigger had considerably better selectivity than the topology trigger. The ZDCs have sufficient energy resolution to count the number of neutrons emitted by the outgoing gold nuclei. We distinguish among several different excitation modes: $XnXn$, in which at least one neutron is detected in each of the ZDC detectors, $1n1n$, in which exactly one neutron is detected in each of the ZDC detectors, $0nXn$, in which at least one neutron is detected in one of the ZDC detectors and none in the other, and $0n0n$, in which no neutrons are detected in either ZDC. The last two modes are only accessible with the topology trigger. A typical ZDC spectrum is shown in Fig. 2. In the west ZDC, the ratio of $1n : 2n : 3n$ is $1 : 0.48 \pm 0.07 : 0.42 \pm 0.04$, whereas in the east ZDC, we find that $1n : 2n : 3n$ is $1 : 0.46 \pm 0.08 : 0.42 \pm 0.04$. This spectrum allows us to measure the cross section for different excitation states.

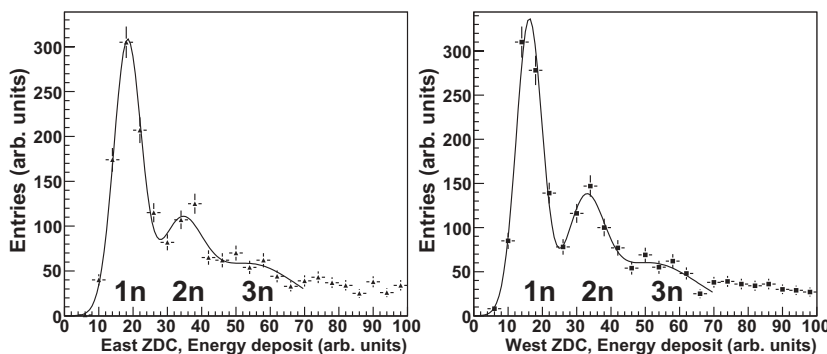FIG. 2. ZDC spectra obtained with the minimum bias sample after the ρ^0 selection cuts are applied and fit with three Gaussians. The east ZDC is shown on the left and the west ZDC is shown on the right. The ratio of numbers of candidates in the west ZDC of $1n : 2n : 3n$ is $1 : 0.48 \pm 0.07 : 0.42 \pm 0.04$, whereas in the east ZDC, we find that $1n : 2n : 3n$ is $1 : 0.46 \pm 0.08 : 0.42 \pm 0.04$.

III. ρ^0 PHOTOPRODUCTION

A. Event selection

This analysis selected events with two oppositely charged tracks forming a primary vertex (beam interaction point) and having less than six reconstructed charged tracks per event. A ρ^0 photoproduction event should have exactly two tracks in the TPC, but additional tracks may come from overlapping interactions, including beam-gas events. The STAR TPC has a 36-μs drift time, so any charged particles traversing the TPC within ±36 μs may deposit energy that overlaps with the tracks of interest. We accounted for the effect of these tracks in our analysis by allowing for varying numbers of total tracks in the event, including primary and secondary tracks. We analyze only events with exactly two tracks forming a primary vertex. If the cut on the total number of tracks is relaxed from two to five, the number of reconstructed ρ^0 increases by $27 \pm 1\%$. The results were corrected by this factor. At the same time, the background increases by a factor of 2.6 ± 0.3; this factor is included in our calculations.

The reconstruction software formed a vertex from the charged particle trajectories. An iterative procedure was used to successively remove tracks that were inconsistent with the vertex position; after the least consistent track was removed, a new vertex was found. This process continued until a vertex was found with an acceptable probability. The single track reconstruction efficiency for $|\eta| < 1.2$ is about 85%, and the vertex-finding efficiency for a two-track vertex is $80 \pm 2\%$. There are several types of backgrounds: peripheral hadronic interactions, other photonuclear interactions, e^+e^- pairs from two-photon interactions, and unrelated processes such as beam-gas interactions, cosmic-ray muons, and pile-up events. These backgrounds can be reduced by cuts on the total multiplicity, vertex position, and other event characteristics.

The multiplicity cut suppresses the contribution from hadronic and pile-up events. After the cuts on the multiplicity, the minimum bias and topology samples contain 48,670 and 98,112 events, respectively. To reduce the backgrounds originating from processes such as beam-gas events, upstream interactions, cosmic rays, and pile-up events, we selected events with primary vertices within 15 cm radially and 100 cm longitudinally (along the beam direction) of the center of the interaction region. Those two cuts reject approximately 25% of the events. We also required that tracks have at least 14 hits in the TPC (out of a maximum of 45 possible hits). This cut rejected another 30% of the events. To retain as many of the incoherently produced ρ^0 mesons as possible while removing combinatorial background, a relatively soft cut on the ρ^0 transverse momentum ($p_T \leqslant 550$ MeV/c) was applied. After cuts, the minimum bias sample contains 5011 events, and the topology sample contains 14,693 events.

Backgrounds from two-photon interactions and non-ρ^0 photonuclear interactions are small. The cross sections for two-photon production of e^+e^- in the STAR acceptance are small [21]. They comprised a small correction in the 130-GeV analysis, but the current study requires $M_{\pi^+\pi^-} > 500$ MeV/c^2. With this cut, the corrections are negligible.

There is also a small background from coherent ω photoproduction; the $\pi^+\pi^-$ final state has a negligible 2.2% branching ratio [22], but the $\pi^+\pi^-\pi^0$ final state has an 89% branching ratio. The ($\pi^+\pi^-$) invariant mass distribution from three-pion decay peaks at a lower value and has a higher p_T than the $\rho^0 \to \pi^+\pi^-$. This is about a 2.7% correction to the incoherent ρ^0 cross section; we neglect this here.

The hadronic interactions produce much higher multiplicity final states than the photoproduced ρ^0 and can be easily distinguished by their total multiplicity [23].

Even with the veto from the top and bottom CTB quadrants in the trigger, some cosmic rays remain in the topology sample. Particles that pass near the interaction region may be reconstructed as a pair of back-to-back tracks with net charge 0, net $p_T \approx 0$, and $y_{\rho^0} \approx 0$. These events are removed by applying a cut on the rapidity so that the accepted events have $|y_{\rho^0}| > 0.01$. However, the ZDC energy coincidence requirements largely eliminate cosmic-ray contamination in the minimum bias sample.

We use two approaches to estimate the remaining backgrounds. As with the 130-GeV analysis, like-sign pairs ($\pi^+\pi^+$ and $\pi^-\pi^-$) provide a good background model [11]. That analysis only considered coherent ρ^0 production; the like-sign background was scaled up by a factor of 2.2 to match the data at high p_T. By definition, this treats incoherent ρ^0 production as a background. We use this approach to measure the ratio of directly produced $\pi^+\pi^-$ pairs to ρ^0 production ($|B/A|$ ratio) for the coherently produced ρ^0 mesons, since it correctly estimates the combinatorial background.

For the rest of the measurements, we use the unscaled background to retain the incoherent ρ^0 signal. For incoherent ρ^0 photoproduction, we split the invariant mass histogram into different p_T ranges, and fit each p_T bin separately to determine the yield. In our fits to the $M_{\pi^+\pi^-}$ spectrum the background is parametrized by a polynomial. The polynomial function is fixed with parameters obtained from the fit of the polynomial function to the nonscaled like-sign distribution. These different approaches for the background description cause a 3% systematic error in the cross-section measurement.

B. Efficiency and acceptance determination

The acceptance of the detector was studied by using a Monte Carlo event generator, which is based on the KN model [5,12], to generate events that reproduce the kinematic properties and spatial distributions of the ρ^0 mesons produced via coherent photoproduction. These events were passed through a realistic detector simulation that reproduces detector resolution and efficiency. The efficiency includes the detector acceptance, track and vertex reconstruction efficiencies, and selection cuts.

The ρ^0 reconstruction efficiency was studied as a function of p_T, p_T^2, Φ (azimuthal angle in the center-of-mass system of Au-Au), Θ (polar angle in the center-of-mass system of Au-Au), y_{ρ^0} (rapidity), and $M_{\pi^+\pi^-}$. The mean efficiency for minimum bias ρ^0s with $|y_{\rho^0}| < 1$ is $44 \pm 2\%$. This efficiency is relatively constant with respect to p_T and azimuthal angle, but it drops as $|y_{\rho^0}|$ increases, owing to the TPC acceptance dropping at higher rapidity. The mean efficiency for topology-triggered ρ^0s with $|y_{\rho^0}| < 1$ is $11 \pm 1\%$; the efficiency drops

slowly as p_T or $|y_{\rho^0}|$ rises. There is also an azimuthal dependence because of the topology trigger veto regions.

The estimated resolution for p_T, y_{ρ^0}, and $M_{\pi^+\pi^-}$ are approximately 6 MeV/c, 0.01, and 6 MeV/c^2, respectively, for track pairs that passed through the ρ^0 selection cuts.

C. Luminosity

The luminosity for the minimum bias data sample is calculated by assuming that the main contribution to the total cross section arises from hadronic production, with a known cross section. The luminosity was measured by counting events with at least 14 primary tracks with $p_T \geqslant 0.1$ GeV/c and $|y_{\rho^0}| \leqslant 0.5$. These events correspond to 80% of the total hadronic production cross section of 7.2 b [24]. An extra correction is required to remove the effects of an unstable dead time caused by the Silicon Vertex Tracker (SVT). The integrated luminosity of the minimum bias sample is measured to be $L = 461$ mb^{-1} with a systematic uncertainty of 10%, which is largely due to the uncertainty of the gold-gold hadronic cross section.

D. Invariant mass fit function

The invariant mass distribution of track pairs was found by assuming that all reconstructed particles were pions; no particle identification was needed owing to the low background level after selection cuts were applied to the tracks. The invariant mass distributions for the minimum bias and topology samples are shown in Fig. 3. Pion pairs may be photoproduced via an intermediate ρ^0, or the photon may fluctuate directly to a $\pi^+\pi^-$ pair. The direct process produces a flat $M_{\pi^+\pi^-}$ mass distribution. The two experimentally indistinguishable processes interfere and the interference is constructive for $M_{\pi^+\pi^-} < M_{\rho^0}$ and destructive for $M_{\pi^+\pi^-} > M_{\rho^0}$ [25].

The invariant mass distribution of the ρ^0 candidates was fit with a relativistic Breit-Wigner [26] function plus a contribution for the direct $\pi^+\pi^-$ production and an interference (Söding) term [27,28]. The background is described by a second-order polynomial. An estimate of the background from the like-sign pairs was used to obtain the parameters for the polynomial function.

The fit function is

$$\frac{dN}{dM_{\pi^+\pi^-}} = \left| A\frac{\sqrt{M_{\pi^+\pi^-}M_{\rho^0}\Gamma_{\rho^0}}}{M_{\pi^+\pi^-}^2 - M_{\rho^0}^2 + iM_{\rho^0}\Gamma_{\rho^0}} + B \right|^2 + f_p, \quad (3)$$

where

$$\Gamma_{\rho^0} = \Gamma_0 \cdot (M_{\rho^0}/M_{\pi^+\pi^-})$$
$$\times \left[(M_{\pi^+\pi^-}^2 - 4m_\pi^2)/(M_{\rho^0}^2 - 4m_\pi^2) \right]^{3/2} \quad (4)$$

is the momentum-dependent width of the ρ^0 and M_{ρ^0} is the mass of the ρ^0, A is the amplitude for the Breit-Wigner function, B is the amplitude for the direct $\pi^+\pi^-$ production, and f_p is the fixed second-order polynomial used to describe the background. For the minimum bias data set, $\Gamma_{\rho^0} = 0.162 \pm 0.007$ GeV/c^2 and $M_{\rho^0} = 0.775 \pm 0.003$ GeV/c^2 from the fit. These values are in good agreement with the PDG [22] values. The difference between the yield obtained with fixed ρ^0 width and mass position from that obtained without
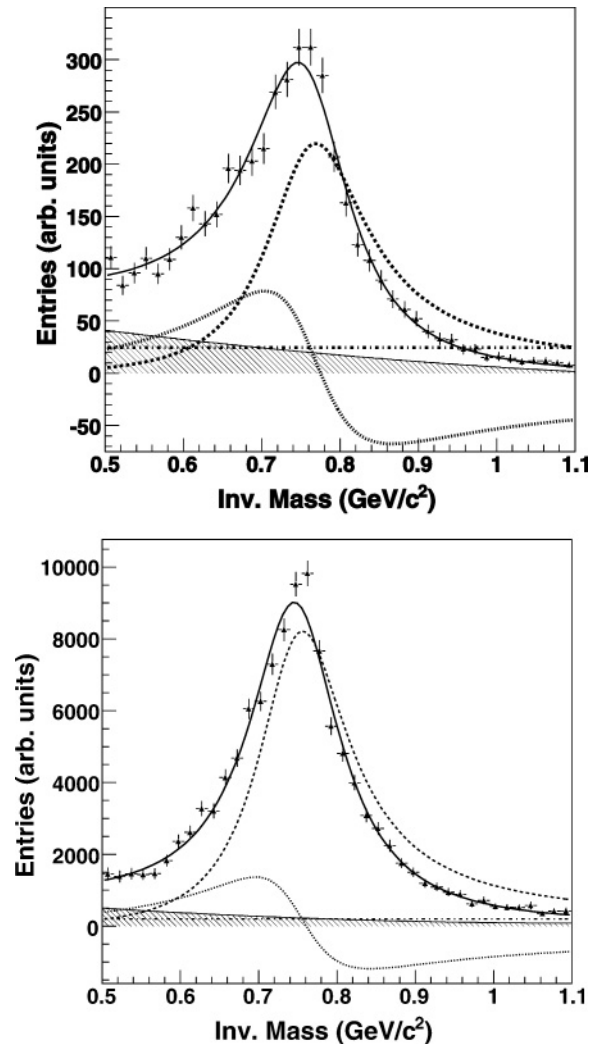

FIG. 3. Top: The invariant mass distribution for the coherently produced ρ^0 candidates from the minimum bias sample with the cut on the ρ^0 transverse momentum $p_T < 150$ MeV/c. Bottom: The invariant mass distribution for the coherently produced ρ^0 candidates obtained from the topology sample with the cut on the ρ^0 transverse momentum $p_T < 150$ MeV/c. The hatched area is the contribution from the combinatorial background. The solid line corresponds to Eq. (3), which encompasses the Breit-Wigner part (dashed), the mass-independent contribution from the direct $\pi^+\pi^-$ production (dash-dotted), and the interference term (dotted).

fixing the width and mass is about 2%. Fixing the width leads to an increase in the χ^2/DOF of 5%. By using the aforementioned fit procedure, the minimum bias sample contains $(3075 \pm 128)\rho^0$ candidates, and the topology sample contains $(13,054 \pm 124)\rho^0$ candidates.

For the minimum bias data, the measured value of $|B/A|$ is 0.89 ± 0.08 (stat.) ± 0.09 (syst.) (GeV/$c)^{-1/2}$; the systematic error from the background description is 3%. Figure 4 shows that $|B/A|$ does not vary significantly as a function of rapidity. Since rapidity is related to photon energy [Eq. (1)] this also shows that there is no significant variation with photon energy. The same energy independence was seen by the ZEUS experiment at HERA [26] and is expected in Pomeron
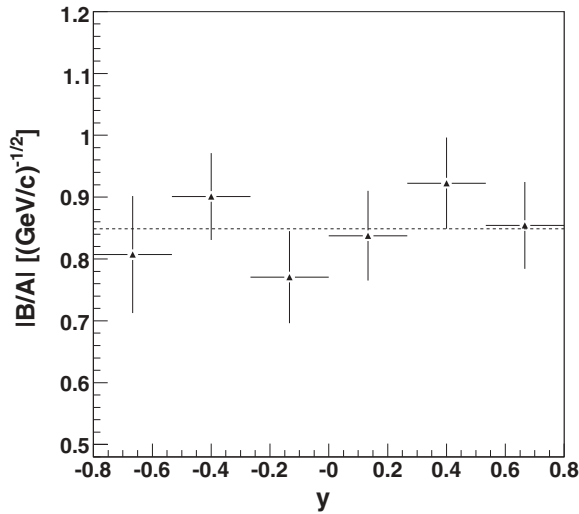
FIG. 4. The ratio $|B/A|$ as a function of y_{ρ^0} for the minimum bias data, obtained by fitting Eq. (3) to the invariant mass distributions in bins of y_{ρ^0}.
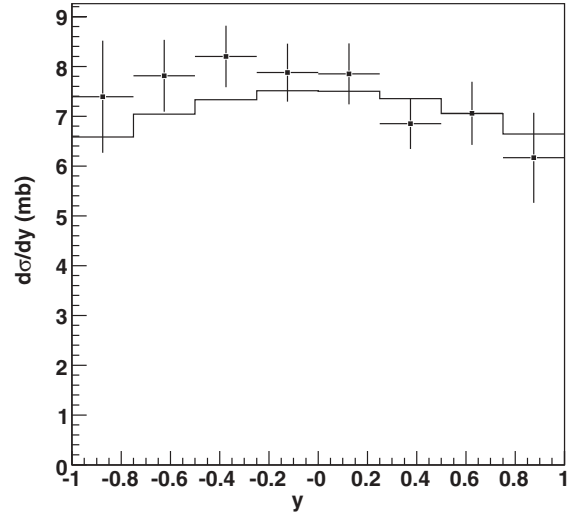

FIG. 5. Coherent ρ^0 production cross section for the minimum bias data set as a function of y_{ρ^0} (black dots) overlaid by the $d\sigma/dy$ distribution predicted by the KN model [23] (solid line).

exchange. In contrast, at lower energies [9], the direct $\pi^+\pi^-$ component decreased as W rose. The difference may be due to ρ production by meson exchange; the meson exchange component is expected to be negligible at RHIC energies. The observed $|B/A|$ ratio is independent of the polar and azimuthal angle, as expected. The slight asymmetry in the distribution is believed to be due to differences between the two parts of the STAR TPC and is included within the systematic uncertainties.

Our measured value for $|B/A|$ is in agreement with the 130-GeV STAR result, $|B/A| = 0.81 \pm 0.08$ (stat.) ± 0.20 (syst.) (GeV/c)$^{-1/2}$ [11]. The ZEUS studies of $\gamma p \rightarrow \rho^0 p$ find $|B/A| = 0.67 \pm 0.03$ (GeV/c)$^{-1/2}$ [26], but for a slightly different kinematic interval. The ZEUS results are for a momentum transfer squared of $t < 0.5$ (GeV/c)^2. At midrapidity in a collider environment, the longitudinal momentum transfer squared from the target nucleus, $t_{||} = (m_V^2/2E_\gamma)^2$, is small [$\approx 2$ (MeV/c)^2]. Therefore $t \approx t_\perp \approx p_T^2$ and so we can extrapolate the ZEUS measurement of the t dependence of $|B/A|$ down to our average value of $t \approx p_T^2 < 0.015$ (GeV/c)^2. Extrapolating the ZEUS results, we find $|B/A| \approx 0.8$, which is consistent with our results. The decrease of $|B/A|$ with increasing $|t|$ and the independence of the polar and azimuthal angles is expected under the assumption that the form factor of the vector meson depends only on t and so no $\sqrt{s_{NN}}$ dependence is expected [25].

In the rest of this paper, we will quote our results in terms of momentum transfer squared, t.

E. Cross sections $d\sigma/dy$ and $d^2\sigma/dydt$ for minimum bias events

The differential cross section as a function of rapidity for ρ^0 photoproduction ($d\sigma/dy$) obtained with the minimum bias sample is shown in Fig. 5. The distribution for each rapidity bin was fit with Eq. (3) and the ρ^0 yield extracted. Also shown is a prediction of the KN model; the other two models do not include nuclear excitation.

Figure 6 shows the ρ^0 spectrum as a function of t for minimum bias data. The efficiency correction and luminosity normalization have been applied.

We do not observe the dip in the range $0.01 < t < 0.015$ (GeV/c)^2 predicted by FSZ [7]. The p_T of the ρ^0 meson is the vector sum of the photon p_T and the p_T transferred by the target nucleus. Since the direction of the photon and scattering p_T are uncorrelated, this addition smears out the diffractive dips [29].

The $d^2\sigma/dydt$ distribution (averaged over $|y_{\rho^0}| < 1$) is fit to a sum of two exponentials, which correspond to coherent and incoherent production:

$$\frac{d^2\sigma}{dydt} = A_{coh} \exp(-B_{coh}t) + A_{inc} \exp(-B_{inc}t). \quad (5)$$
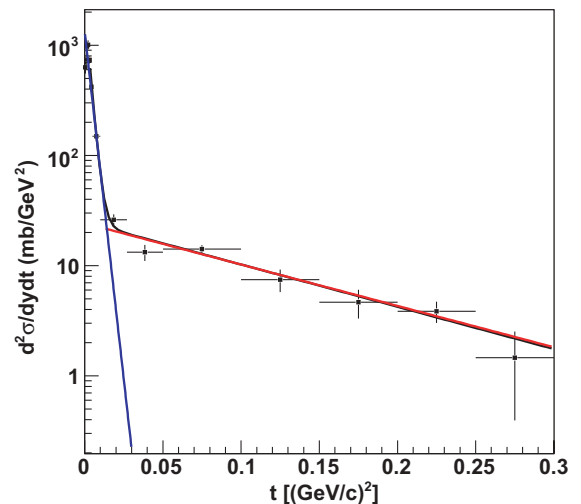

FIG. 6. (Color online) ρ^0 production cross section as a function of the momentum transfer squared, t, together with the fit of Eq. (5). The fit parameters are shown in Table I.

TABLE I. Parameters for the fit to $d^2\sigma/dydt$, Eq. (5).

Parameter	t range (0., 0.3) $(GeV/c)^2$	t range (0.002, 0.3) $(GeV/c)^2$
A_{coh}, mb/$(GeV/c)^2$	1050 ± 57	2307 ± 258
B_{coh}, $(GeV/c)^{-2}$	256 ± 12	388 ± 24
A_{inc}, mb/$(GeV/c)^2$	21.6 ± 2.4	24.8 ± 2.5
B_{inc}, $(GeV/c)^{-2}$	7.9 ± 0.9	8.8 ± 1.0

The simple fit function shown in Eq. (5) has two drawbacks. The interference between ρ^0 photoproduction on the two nuclei reduces $d^2\sigma/dydt$ at small t [12,29] and, in fact, alters the minimum bias t spectrum at the 20% level for $t < 0.01$ $(GeV/c)^2$.

A fit over all t values yields exponentials (shown in the left column of Table I) that are integrable to give the total coherent cross section (although note that given are the parameters of the exponentials, not the cross section). Because of the interference at small t, this fit has a poor χ^2/DOF of 79.12/10. A second fit (shown in the right column of Table I) is performed over the t range from 0.002 to 0.3 $(GeV/c)^2$. It avoids the region where the interference is large and has a χ^2/DOF of 8.1/7. This fit yields a nuclear slope with accuracy comparable to other experiments. Both fits give similar results for the incoherent production.

The incoherent slope, $B_{inc} = 8.8 \pm 1.0$ $(GeV/c)^{-2}$ has not previously been determined in heavy ion collisions. However, it is comparable to the slope observed by STAR in dAu collisions [30] and comparable to the ZEUS result $B_p = 10.9 \pm 0.3$ (stat.)$^{+1.0}_{-0.5}$ (syst.) $(GeV/c)^{-2}$ [26] and H1 result $B_p = 10.9 \pm 2.4$ (stat.) ± 1.1 (syst.) $(GeV/c)^{-2}$ [31] for ρ^0 photoproduction on proton targets at comparable t values. The HERA data are at higher $W_{\gamma N}$, but the energy difference is not expected to introduce a large shift.

With the second fit region we find the coherent production slope of $B_{coh} = 388 \pm 24$ $(GeV/c)^{-2}$, obtained with the double-exponential fit function. For direct comparison with the previous STAR result, we also performed a single exponential fit, which gave $B_{coh} = 363 \pm 21$ $(GeV/c)^{-2}$, in agreement with the value observed at 130 GeV, 358 ± 31 $(GeV/c)^{-2}$ [11]. These numbers are not directly comparable with fixed-target photoproduction data because the photon flux in UPC photoproduction is higher on the side of the target nearest the photon emitter and lower on the far side of the target. The photon flux falls as $1/r^2$, which leads to a slightly smaller apparent source size.

Despite these difficulties, the two exponentials in Eq. (5) were integrated analytically to find the total coherent and incoherent cross sections. This approach neglects the corrections from the loss of incoherent cross section when the coherent cross section is large [32], but it is useful for phenomenological comparisons. For $|y_{\rho^0}| < 1$, we find the ratio

$$\sigma_{incoherent}/\sigma_{coherent} = 0.29 \pm 0.03(\text{stat.}) \pm 0.08(\text{syst.})$$

for events with mutual excitation ($XnXn$).

We have also studied the cross sections for ρ^0 production accompanied by single-neutron emission ($1n1n$),
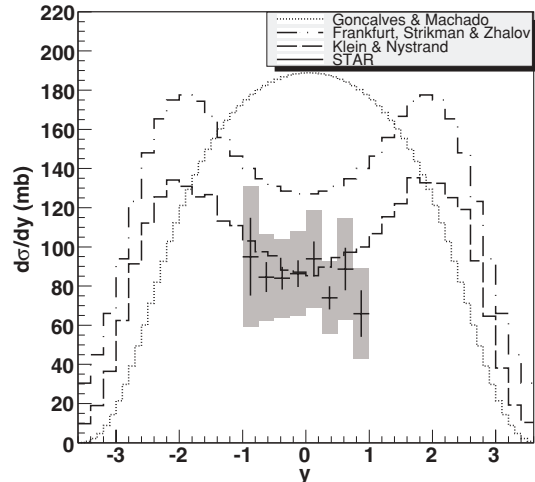

FIG. 7. Comparison of theoretical predictions to the measured differential cross section for coherent ρ^0 production. The statistical errors are shown by the solid vertical line at each data point. The sum of the statistical and systematic error bars is shown by the gray band.

which is largely due to mutual excitation of GDRs. We did this by fitting the ZDC spectra in Fig. 2 and extracting the single-neutron component from the fit. For $|y_{\rho^0}| < 1$, we find $\sigma_{incoherent}^{1n1n}/\sigma_{coherent}^{1n1n} = 0.18 \pm 0.08$ (stat.) ± 0.05 (syst.). The higher $\sigma_{incoherent}/\sigma_{coherent}$ for the $XnXn$ sample may signal a breakdown of the factorization implicit in Eq. (2) because the incoherent ρ^0 production transfers enough energy to disassociate the target nucleus. This effect would lead to additional multiple neutron emission [33].

F. Total cross sections

We have compared three theoretical models to our measurements [5,6,8]. The comparison is shown in Fig. 7.

The total production cross section, $d\sigma_{tot}/dy$, is obtained by scaling the mutual excitation results with the scaling factors $\sigma(\rho^0_{0n0n})/\sigma(\rho^0_{XnXn})$ and $\sigma(\rho^0_{0nXn})/\sigma(\rho^0_{XnXn})$ as a function of rapidity. The scaling is needed because the efficiency of the topology trigger, which enters into the total cross section, is only poorly known. Therefore the ρ^0 production cross section for the events with mutual excitation ($XnXn$) measured with the minimum bias sample was extrapolated based on the ratios $\sigma(0n0n)/\sigma(XnXn) = 7.1 \pm 0.3$ (stat.) and $\sigma(0nXn)/\sigma(XnXn) = 3.5 \pm 0.2$ (stat.), which are measured within the topology sample. Because of the limited acceptance in rapidity, we cannot distinguish the different theoretical models based on the shape. However, the amplitude can be used to eliminate models that significantly overestimate the total production cross section in the measured rapidity range.

The cross sections for coherent and incoherent production for $|y_{\rho^0}| < 1$ accompanied by nuclear excitation are $\sigma_{coh}(XnXn, |y_{\rho^0}| < 1) = 14.5 \pm 0.7$ (stat.) ± 1.9 (syst.) mb and $\sigma_{inc}(XnXn, |y_{\rho^0}| < 1) = 4.5 \pm 0.5$ (stat.) ± 0.6 (syst.) mb.

Finding the total cross sections requires an extrapolation to the region $|y_{\rho^0}| > 1$. This extrapolation is necessarily model dependent. The KN [23] and FSZ [7] calculations have similar

TABLE II. The total cross section extrapolated to the full rapidity range for coherent ρ^0 production at $\sqrt{s_{NN}} = 200$ GeV accompanied by nuclear breakup and without breakup compared with previous measurements at $\sqrt{s_{NN}} = 130$ GeV [11]. The first error is statistical; the second is systematic.

Parameter	STAR at $\sqrt{s_{NN}} = 130$ GeV	STAR at $\sqrt{s_{NN}} = 200$ GeV	STAR at $\sqrt{s_{NN}} = 200$ GeV
	coherent	coherent	coherent + incoherent
$\sigma_{XnXn}^{\rho^0}$ (mb)	$28.3 \pm 2.0 \pm 6.3$	$31.9 \pm 1.5 \pm 4.5$	$41.4 \pm 2.9 \pm 5.8$
$\sigma_{0nXn}^{\rho^0}$ (mb)	$95 \pm 60 \pm 25$	$105 \pm 5 \pm 15$	$145 \pm 7 \pm 20$
$\sigma_{1n1n}^{\rho^0}$ (mb)	$2.8 \pm 0.5 \pm 0.7$	$2.4 \pm 0.2 \pm 0.4$	$2.8 \pm 0.3 \pm 0.4$
$\sigma_{0n0n}^{\rho^0}$ (mb)	$370 \pm 170 \pm 80$	$391 \pm 18 \pm 55$	$508 \pm 24 \pm 71$
$\sigma_{\text{total}}^{\rho^0}$ (mb)	$460 \pm 220 \pm 110$	$530 \pm 19 \pm 57$	$697 \pm 25 \pm 73$

$d\sigma_{\text{tot}}/dy$ distributions and so a single extrapolation should work well for them. For the KN calculation, the extrapolation factor from $\sigma(|y_{\rho^0}| < 1)$ to σ_{tot} is 2.2 ± 0.1 for the events with nuclear breakup. We assume that this factor is the same for coherent and incoherent production. The coherent production cross section extrapolated to the full rapidity range is $\sigma_{\text{coh}}(XnXn, \text{full-}y) = 31.9 \pm 1.5$ (stat.) ± 4.5 (syst.) mb. The total cross section is

$$\sigma_{\text{coh+inc}}(XnXn, \text{full-}y) = 41.4 \pm 2.9 \text{ (stat.)} \pm 5.8 \text{ (syst.) mb,}$$

where the $XnXn$ denotes multiple neutron emission from nuclear dissociation.

For ρ^0 production accompanied by single-neutron emission, we find, $\sigma_{\text{coh}}(1n1n, |y_{\rho^0}| < 1) = 1.07 \pm 0.08$ (stat.) $\pm$ 0.14 (syst.) mb and $\sigma_{\text{inc}}(1n1n, |y_{\rho^0}| < 1) = 0.21 \pm 0.09$ (stat.) ± 0.03 (syst.) mb.

The extrapolation factor from $|y_{\rho^0}| < 1$ to 4π is assumed to be the same as that for the $XnXn$ data set (i.e., 2.2). The total cross section for single-neutron emission is

$$\sigma_{\text{coh+inc}}(1n1n, \text{full-}y) = 2.8 \pm 0.3 \text{ (stat.)} \pm 0.4 \text{ (syst.) mb.}$$

Based on the ratio $\sigma(\rho^0_{0n0n})/\sigma(\rho^0_{XnXn})$, we find $\sigma_{\text{coh}}(0n0n, |y_{\rho^0}| < 1) = 106 \pm 5$ (stat.) ± 14 (syst.) mb.

As with the $XnXn$ data, the extrapolation to 4π is model dependent. For the KN model, the extrapolation factor is 3.7. For the FSZ model, the factor would be 3.5, and for the saturation model GM [8], it is 2.13. The KN and FSZ model factors are similar, which is remarkable since the predicted cross sections differ by 60%. Since the KN $d\sigma/dy$ matches the $XnXn$ data well, we adopt an overall extrapolation factor of 3.7 ± 0.1. With that, we find $\sigma_{\text{coh}}(0n0n, \text{full-}y) = 391 \pm 18$ (stat.) ± 55 (syst.) mb and a total cross section of events with $0n0n$ (coherent, incoherent) of

$$\sigma_{\text{coh+inc}}(0n0n, \text{full-}y) = 508 \pm 24 \text{ (stat.)} \pm 71 \text{ (syst.) mb.}$$

It is also possible for a single nucleus to be excited ($0nXn$ in this language). The $0nXn$ cross section includes the possibility for either of the two nuclei to dissociate. We have checked that we get symmetric results for this channel when the signals are in the east or west ZDC; those events are added and treated equally.

This yields the total coherent cross section $\sigma_{\text{coh}}(\text{AuAu} \rightarrow \text{Au}^{(*)}\text{Au}^{(*)}\rho^0) = 530 \pm 19$ (stat.) ± 57 (syst.) mb, and total cross section (coherent, incoherent)

$$\sigma_{\text{coh+inc}}(\text{AuAu} \rightarrow \text{Au}^{(*)}\text{Au}^{(*)}\rho^0)$$
$$= 697 \pm 25 \text{ (stat.)} \pm 73 \text{ (syst.) mb.}$$

Table II summarizes the measured coherent and incoherent production cross sections and compares them with results obtained at $\sqrt{s_{NN}} = 130$ GeV [11]. The measured 12% increase (with large errors) in the coherent photoproduction cross section (going from 130- to 200-GeV collisions) is much less than is predicted by all three models (Refs. [6,23], and [8]), which predict cross section increases of between 70% and 80%. Our results at $\sqrt{s_{NN}} = 200$ GeV/c support the ρ^0-nucleon cross sections used in KN [23].

Several sources of systematic error have been considered in this analysis. The main sources of the systematic errors for the cross section in the rapidity range $|y_{\rho^0}| < 1$ are 10% for the luminosity measurement, 3% from the different approaches for the background description, and 7% for the applied cuts and fit function. The major additional systematic error for the total coherent and incoherent production cross sections is 6% for the extrapolation to the full rapidity interval. The error is mainly due to the difference between the extrapolation factor in KN and FSZ models. These uncertainties were added in quadrature to give the systematic error for the total production cross section.

G. ρ^0 spin density matrix

The angular distribution of the π^+ and π^- in the γ-nucleon center-of-mass frame can be used to determine the ρ^0 spin density matrix elements. This has previously been studied in γp collisions at HERA [26]. There, measurement of the recoiling proton allowed the γp center-of-mass frame to be determined. STAR does not observe the recoiling proton, and so we cannot separate the measured p_T into contributions from the photon and from the nucleon. Furthermore, there is a twofold ambiguity about photon direction. Because of these problems, we perform our analysis with respect to the z-axis (beam direction). Since the laboratory frame is heavily
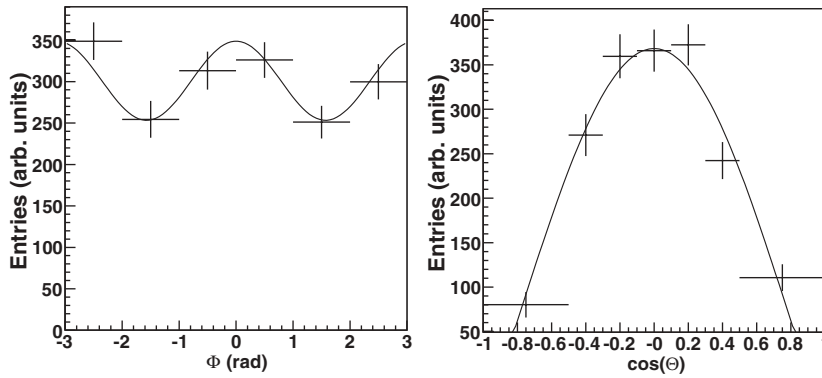
FIG. 8. Projections of the two-dimensional efficiency-corrected Φ_h vs $\cos(\Theta_h)$ distributions obtained with the minimum bias data set. The solid line shows the result of the two-dimensional fit to the data with Eq. (6) and the coefficients given in Table III.

boosted with respect to the γp center-of-mass frame, this is a good approximation; in the target frame, the ρ^0 direction is within 1–2 mrad of the beam axis. Θ_h is defined as the polar angle between the beam direction and the direction of the π^+ in the ρ^0 rest frame. With the twofold ambiguity in photon direction, the $+z$ and $-z$ directions are equivalent. This does not affect two terms—$\cos^2(\Theta_h)$ and $\sin^2(\Theta_h)$—since they are symmetric around $\pi/2$ (i.e., around mid-rapidity). However the term $\sin(2\Theta_h)$ is not symmetric around $\pi/2$ and therefore we are not sensitive to the interference between helicity states nonflip to single flip. The azimuthal angle Φ_h is the angle between the decay plane and the ρ^0 production plane. The production plane of the ρ^0 contains the ρ^0 and a virtual photon. The dependence of the cross section on Φ_h and $\cos(\Theta_h)$ can be written as follows [17]:

$$\frac{1}{\sigma}\frac{d^2\sigma}{d\cos(\Theta_h)d\Phi_h} = \frac{3}{4\pi} \cdot \left[\frac{1}{2}\left(1 - r_{00}^{04}\right)\right.$$
$$+ \frac{1}{2}\left(3r_{00}^{04} - 1\right)\cos^2(\Theta_h)$$
$$- \sqrt{2}\Re e\left[r_{10}^{04}\right]\sin(2\Theta_h)\cos(\Phi_h)$$
$$\left. - r_{1-1}^{04}\sin^2(\Theta_h)\cos(2\Phi_h)\right]. \quad (6)$$

The three independent spin density matrix elements r_{00}^{04}, r_{10}^{04}, and r_{1-1}^{04} can be extracted by fitting the two-dimensional angular correlation. The superscripts indicate contributions from the photon polarization states [34]. The element r_{00}^{04} represents the probability that the ρ^0 is produced with helicity 0 from a photon with helicity ± 1. The element r_{1-1}^{04} is related to the size of the interference between the helicity nonflip and

double flip and $\Re e[r_{10}^{04}]$ is related to the interference of nonflip to single flip, where $\Re e[r_{10}^{04}]$ stands for the real part of r_{10}^{04}. If helicity conservation holds, then all three matrix elements will be close to zero.

Figure 8 shows the Φ_h versus $\cos(\Theta_h)$ correlation fit for the minimum bias data set. The measured spin density matrix elements are shown in Table III. The method used is to fit the invariant mass distributions in bins of Φ_h and $\cos(\Theta_h)$ to determine the yield in each bin.

The background is accounted for in the fitting function with nonscaled like-sign pairs as described in Sec. III A. The main contribution to the systematic uncertainty comes from the background subtraction. It was estimated by using an alternative approach where the scaled invariant mass distribution of the like-sign pairs was subtracted from that of the opposite-sign pairs. An additional source of systematic error is the uncertainty from the acceptance correction determined by a ρ^0 Monte Carlo simulation. We estimate the systematic error by varying the bin size of Φ_h and $\cos(\Theta_h)$. The systematic error for the spin density matrix elements is obtained by adding the individual uncorrelated contributions in quadrature. The measured ρ^0 helicity matrix elements indicate that helicity is conserved within errors, as expected based on s-channel helicity conservation.

IV. CONCLUSION

Photoproduction of ρ^0 mesons has been measured in the STAR detector at RHIC in Au-Au collisions at $\sqrt{s_{NN}} = 200$ GeV. Coherent and incoherent ρ^0 photoproduction has been observed and photoproduction of the ρ^0 mesons is observed with and without accompanying Coulomb nuclear excitations. The measured increase with energy in the total cross section for photoproduction is much slower than proposed in Refs. [7] and [8]. However, the Klein and Nystrand model [5] is able to describe the data for two energy points, $\sqrt{s_{NN}} = 130$ and 200 GeV.

The differential cross section for photoproduction has been studied as a function of t, y_{ρ^0}, and $M_{\pi^+\pi^-}$. The $d^2\sigma/dy\,dt$ distribution was fit with a double-exponential function to isolate the incoherent part of the ρ^0 production cross section.

The ratio of $\pi^+\pi^-$ to direct ρ^0 production ($|B/A|$) has been studied with respect to polar angle, azimuthal angle, and y_{ρ^0}; no dependence has been observed, as predicted in Ref. [25].

TABLE III. Measured spin density matrix elements compared with ZEUS(γp) results. The first error is statistical; the second is systematic.

Parameter	Fit result	γp experiment [26]
χ^2/ndf	26/21	
r_{00}^{04}	$-0.03 \pm 0.03 \pm 0.06$	$0.01 \pm 0.01 \pm 0.02$
$\Re e[r_{10}^{04}]$	–	$0.01 \pm 0.01 \pm 0.01$
r_{1-1}^{04}	$-0.01 \pm 0.03 \pm 0.05$	$-0.01 \pm 0.01 \pm 0.01$

The r_{00}^{04} and r_{1-1}^{04} spin density matrix elements for the ρ^0 meson were measured. The small values of r_{00}^{04} and r_{1-1}^{04} indicate that helicity is conserved within errors, as expected based on s-channel helicity conservation, and therefore we see no evidence for ρ^0 photoproduction involving spin flip.

[1] G. Baur *et al.*, Phys. Rep. **364**, 359 (2002); F. Krauss, M. Greiner, and G. Soft, Prog. Part. Nucl. Phys. **39**, 503 (1997).

[2] C. Bertulani, S. Klein, and J. Nystrand, Annu. Rev. Nucl. Part. Sci. **55**, 271 (2005).

[3] C. F. v. Weizsäcker, Z. Phys. **88**, 612 (1934); E. J. Williams, Phys. Rev. **45**, 729 (1934).

[4] J. R. Forshaw and D. A. Ross, *Quantum Chromodynamics and the Pomeron* (Cambridge University Press, Cambridge, UK, 1997).

[5] S. R. Klein and J. Nystrand, Phys. Rev. C **60**, 014903 (1999).

[6] L. Frankfurt, M. Strikman, and M. Zhalov, Phys. Rev. C **67**, 034901 (2003).

[7] L. Frankfurt, M. Strikman, and M. Zhalov, Phys. Lett. **B537**, 51 (2002).

[8] V. P. Gonçalves and M. V. T. Machado, Eur. Phys. J. C **40**, 519 (2005).

[9] F. Bulos *et al.*, Phys. Rev. Lett. **22**, 490 (1969); H. Alvensleben *et al.*, Phys. Rev. Lett. **24**, 786 (1970); **24**, 792 (1970); Nucl. Phys. **B18**, 333 (1970); G. McClellan *et al.*, Phys. Rev. D **4**, 2683 (1971); D. Aston *et al.*, Nucl. Phys. **B209**, 56 (1982).

[10] D. d'Enterria (for the PHENIX Collaboration), nucl-ex/0601001.

[11] C. Adler *et al.*, Phys. Rev. Lett. **89**, 272302 (2002).

[12] A. J. Baltz, S. R. Klein, and J. Nystrand, Phys. Rev. Lett. **89**, 012301 (2002).

[13] G. Baur *et al.*, Nucl. Phys. **A729**, 787 (2003).

[14] C. Adler *et al.*, Nucl. Instrum. Methods A **470**, 488 (2001).

[15] G. Baur and C. A. Bertulani, Phys. Lett. **B174**, 23 (1986).

[16] F. J. Gilman *et al.*, Phys. Lett. **B31**, 387 (1970).

[17] K. Schilling *et al.*, Nucl. Phys. **B15**, 397 (1970); K. Schilling and G. Wolf, Nucl. Phys. **B61**, 381 (1973).

[18] A. Airapetian *et al.*, Phys. Lett. **B513**, 301 (2001); M. R. Adams *et al.* (E665 Collaboration), Z. Phys. C **74**, 237 (1997); W. D. Shambroom *et al.* (CHIO Collaboration), Phys. Rev. D **26**, 1 (1982).

[19] M. Anderson *et al.*, Nucl. Instrum. Methods A **499**, 659 (2003); M. Anderson *et al.*, Nucl. Instrum. Methods A **499**, 679 (2003).

[20] F. S. Bieser *et al.*, Nucl. Instrum. Methods A **499**, 766 (2003).

[21] J. Adams *et al.*, Phys. Rev. C **70**, 031902(R) (2004).

[22] W.-M. Yao *et al.*, J. Phys. G: Nucl. Part. Phys. **33**, 1 (2006).

[23] J. Nystrand and S. Klein, LBNL Report 42524, nucl-ex/9811007.

[24] A. J. Baltz, C. Chasman, and S. N. White, Nucl. Instrum. Methods A **417**, 1 (1998).

[25] M. G. Ryskin and Yu. M. Shabelski, Yad. Fiz. **61**, 89 (1998).

[26] J. Breitweg *et al.*, Eur. Phys. J. C **2**, 247 (1998).

[27] P. Söding, Phys. Lett. **19**, 702 (1966).

[28] J. J. Sakurai, Ann. Phys. (NY) **11**, 1 (1960); T. H. Bauer *et al.*, Rev. Mod. Phys. **50**, 261 (1978).

[29] S. R. Klein and J. Nystrand, Phys. Rev. Lett. **84**, 2330 (2000).

[30] S. Timoshenko (for the STAR Collaboration), nucl-ex/0701077.

[31] S. Aid *et al.* (H1 Collaboration), Nucl. Phys. **B463**, 3 (1996).

[32] G. V. Bochmann, B. Margolis, and C. L. Tang, Phys. Lett. **B30**, 254 (1969).

[33] M. Strikman, M. Tverskoy, and M. Zhalov, Phys. Lett. **B626**, 72 (2005).

[34] J. Breitweg *et al.*, Eur. Phys. J. C **12**, 393 (2000).